Neptunium(V) sorption to goethite at attomolar to micromolar concentrations

Mathew S. Snow [a,b,*], Pihong Zhao [a], Zurong Dai [a], Annie B. Kersting [a], Mavrik Zavarin [a]

[a] Glenn T. Seaborg Institute, Physical and Life Sciences Directorate, Lawrence Livermore National Laboratory, PO Box 808, Livermore, CA 94550, USA
[b] Department of Chemistry, Washington State University, PO Box 644630, Pullman, WA 99164-4630, USA

ARTICLE INFO

ABSTRACT

Sorption of 10^{-18}–10^{-5} M neptunium (Np) to goethite was examined using liquid scintillation counting and gamma spectroscopy. A combination approach using ^{239}Np and long lived ^{237}Np was employed to span this wide concentration range. ^{239}Np detection limits were determined to be 2×10^{-18} M and 3×10^{-17} M for liquid scintillation counting and gamma spectroscopy, respectively. Sorption was found to be linear below 10^{-11} M, in contrast to the non-linear behavior observed at higher concentrations both here and in the literature. 2-site and 3-site Langmuir models were used to simulate sorption behavior over the entire 10^{-18}–10^{-5} M range. The 3-site model fit yielded Type I and II site densities of 3.56 sites/nm^2 (99.6%) and 0.014 ± 0.007 sites/nm^2 ($0.4 \pm 0.1\%$), consistent with typical "high affinity" and "low affinity" sites reported in the literature [21]. Modeling results for both models suggest that sorption below ${\sim}10^{-11}$ M is controlled by a third (Type III) site with a density on the order of ${\sim}7 \times 10^{-5}$ sites/nm^2 (${\sim}0.002\%$). While the nature of this "site" cannot be determined from isotherm data alone, the sorption data at ultra-low Np concentrations indicate that Np(V) sorption to goethite at environmentally relevant concentrations will be (1) linear and (2) higher than previous (high concentration) laboratory experiments suggest.

1. Introduction

Kilogram quantities of Np have been introduced into the environment as a result of nuclear weapons testing and nuclear power [1–4]. While initially present in relatively small quantities in spent nuclear fuel (0.02–0.1%) [5], its in-growth from ^{241}Am, coupled with its long half life (2.14×10^6 yrs) and relatively weak sorption, results in ^{237}Np becoming a major dose contributor in a geological repository after 10,000 years [6,7].

Under oxidizing conditions prevalent throughout much of the subsurface, Np exists primarily in the pentavalent oxidation state [6]. As a result of the low charge/size ratio of its dominant cationic species in aqueous solutions (NpO_2^+), Np(V) sorbs weakly to most mineral surfaces and is thus expected to be the most environmentally mobile actinide [8,9].

Np(V) sorption to mineral surfaces can both retard as well as increase migration. Np(V) is effectively removed from the mobile phase if it is sorbed to immobile minerals in soil or on fracture surfaces. However, the transport of Np(V) can also be enhanced if sorbed to a mobile colloid [10–12]. Iron oxides are thought to play an important role in the environmental transport of low solubility actinides because of their ubiquity, high metal sorption affinities, and high sorption capacities [13–15]. Thus, understanding the

sorption/desorption behavior of Np to iron oxides is important for developing accurate environmental transport models.

Many of the studies on the sorption of Np have been performed via radiometric counting (i.e. liquid scintillation counting and gamma spectroscopy) of ^{237}Np which, as a result of the long half life of ^{237}Np (2.14×10^6 yrs), has restricted such studies to relatively high aqueous Np concentrations ($>10^{-10}$ M) [8,27–30]. However, Np concentrations in the environment are typically much lower. For example, at the Nevada National Security Site (formerly known as the Nevada Test Site), Np concentrations are routinely measured at 10^{-13}–10^{-17} M in groundwater [31]. Thus, new methods to study the sorption of Np at ultra-low, femto-molar concentrations are necessary.

Several radiotracers for ^{237}Np have been utilized in the literature for low-level environmental Np analyses and include ^{235}Np ($t_{1/2}$ = 396.1 days) [13,32], ^{236}Np ($t_{1/2}$ = 1.54×10^5 yrs) [4], and ^{239}Np ($t_{1/2}$ = 2.3565 days), of which ^{239}Np is most common owing to its much greater availability [7,32–33]. However, to our knowledge only one sorption study using short-lived ^{239}Np isotopes is reported in the literature [7], compared to the many high concentration sorption studies reported using ^{237}Np [18,28–30].

Experimental and modeling studies of metal ion sorption to iron oxides have shown that sorption cannot always be explained as binary adsorption at a single type of surface group or "site". As a result, multi-site sorption models are frequently employed [16–21]. In such models, the iron oxide surface is modeled as

containing a relatively large quantity (~90–99%) of "low affinity" sites which characterize bulk sorption behavior and smaller quantities (~1–10%) of "high affinity" sites which control sorption behavior at low mineral surface loads [21]. Spectroscopic studies suggest that the observed "high affinity" sites can potentially result from heterogeneity in the mineral surface and can include structural features such as "edges" [22,23] and "corners" [22,24] of the iron octahedra, adatom sites [25], and defect sites in the mineral surface. Further variability in the sorption behavior has also been shown to result from differing affinities toward different exposed iron oxide crystal faces [22,23]. However, in the absence of spectroscopic or other information, "sites" identified based on fitting isotherm data do not necessarily imply specific reaction mechanisms [16,34,35].

Studies of Np sorption at moderate concentrations (10^{-6}–10^{-8} M) have suggested Freundlich-like behavior, in that as the Np concentration increases, the distribution coefficient (K_d, defined as the concentration of Np associated with the solid divided by the concentration in the aqueous phase) decreases [18]. Fundamentally, the Freundlich isotherm has been shown to be equivalent to a multi-site Langmuir model in which a Gaussian-like distribution of site affinities exists [47]. Thus, the Freudlich model can be considered an end-member in the multi-site modeling approach. The use of Freundlich isotherms is commonly employed in order to describe experimentally observed increasing K_d values with decreasing sorbate concentration at relatively high concentrations (>10^{-10} M). However, one consequence of the application of a Freundlich model is that K_ds are predicted to continuously increase as the sorbate concentration decreases, resulting in extremely high K_ds when extrapolated to ultra-low concentrations. Observations made by Girvin et al. [13] with respect to Np sorption to amorphous iron oxyhydroxides indicate that Np sorption will transition to linear behavior at trace concentrations (10^{-12}–10^{-14} M). A similar change to linear sorption behavior at low concentrations for Cd, Cu and Zn on amorphous iron oxyhydroxides was observed by Dzombak and Morel [16] and Benjamin and Leckie [26]. It is reasonable to expect that this same transition will occur for Np on goethite. However, the aqueous concentration or surface loading at which this occurs is not known. The objectives of this study were to (1) examine Np–goethite interactions over a wide concentration range (10^{-18}–10^{-5} M) in order to compare Np behavior at high concentrations to Np behavior at ultra-low concentrations more commonly observed in the field, (2) develop a radioanalytical method utilizing ^{239}Np tracers for sorption studies at ultra-low concentrations, and (3) develop a consistent model to describe Np–goethite sorption behavior over a wide range of concentrations and surface loading.

2. Experimental

All chemicals used in this work were ACS reagent grade unless otherwise specified. Goethite was synthesized based on methods described by Schwertman and Cornell [36]. Characterization data of the goethite stock solution used in these experiments was recently reported by Tinnacher et al. [18]. The goethite had a low BET surface area of 15.8 m^2 g^{-1}. The point of zero charge was 8.5 ± 0.1 as determined using the potentiometric titration method.

2.1. Np stock preparations

^{239}Np was purified from an Am stock available at LLNL which contained 90% (by activity) ^{243}Am and 10% ^{241}Am [31]. Briefly, a small aliquot of the Am stock was baked to near dryness and reconstituted in a solution of concentrated HCl + HI (50:1 v/v). Columns

(2 mL, AG BioRad 50–100 mesh resin) were pre-conditioned with several column volumes of HCl + HI prior to loading the stock. Americium was eluted using several column volumes of HCl + HI. The Np fraction was eluted using several column volumes of 6 M HCl + 0.05 M HF.

Maximum purification of ^{239}Np was essential in order to lower the background count rate resulting from two major factors: (1) ^{239}Np in-growth during the sorption experiment resulting from incomplete separation from ^{243}Am, and (2) possible small quantities of ^{237}Np contamination, in-grown from ^{241}Am in the Am stock solution [31]. To minimize the ^{237}Np background, an initial purification of the Am stock solution was performed and the Np fraction discarded (Fig. EA-4). The first usable ^{239}Np separation was performed 24 h later using the Am stock from the initial purification. In addition, the ^{239}Np fraction underwent a second column separation, after which no Am or ^{237}Np was detected by gamma spectroscopy or liquid scintillation counting.

^{237}Np was obtained from a ^{237}Np stock available at LLNL. Separation of ^{237}Np from ^{233}Pa was performed using the procedure of Pickett et al. [37]. Briefly, the stock solution was baked to near dryness and reconstituted in concentrated HCl three times (to drive off an residual HF that may have been initially present in the stock solution). Np was dissolved in 1 mL of HCl + HI. Columns (2 mL, AG BioRad 100–200 mesh resin) were pre-conditioned with several column volumes of concentrated HCl, followed by three column volumes of HCl + HI prior to loading the stock. ^{233}Pa was eluted using five column volumes of 9 M HCl + 0.05 M HF. ^{237}Np was eluted using five column volumes of 6 M HCl + 0.05 M HF. The purified ^{237}Np solution was slowly heated until the volume was reduced to one drop. The procedure was then repeated a second time, resulting in 99 + % pure ^{237}Np solution determined by gamma spectroscopy and liquid scintillation counting.

Oxidation of the purified Np solutions to the +5 and +6 oxidation states was performed by heating the solution and reducing the volumes to one drop and then reconstituting the Np in 5 M HNO$_3$ three times. Reduction to the +5 state was subsequently performed by adding one to three drops of H$_2$O$_2$, covering the solutions, and very lightly heating for ~30 min. Small aliquots of high concentration ^{237}Np solutions were taken and analyzed using a Cary 500 UV–Vis spectrophotometer. The oxidation/reduction cycle was repeated as necessary until 100% of the neptunium was confirmed to be in the Np(V) oxidation state.

For the lowest concentration solutions of pure ^{239}Np, the oxidation state was verified indirectly via extraction chromatography using an EICHROM UTEVA column. Since UTEVA strongly retains actinides in the +4 and +6 state, but not the +5, a pure solution of Np(V) passes un-retained through the column. A small aliquot of the ^{239}Np solution was diluted in 5 M HNO$_3$ and eluted. Liquid scintillation counting showed that 95 ± 10% of the ^{239}Np was collected in the effluent.

2.2. Sorption experiments

All sorption experiments were performed in 5 mM NaCl/0.7 mM NaHCO$_3$ (pH ~ 8) solution prepared by adding appropriate amounts of each salt to 18 MΩ cm H$_2$O and filtering through a 0.45 μm filter. This solution composition was chosen to provide a direct comparison to sorption experiments reported in Tinnacher et al. [18]. Under these solution conditions, aqueous Np(V) speciation is dominated by NpO$_2^+$ as determined using stability constant data from NEA [38] (Fig. EA-5).

For batch sorption experiments, a 20 g/L goethite stock solution was prepared in 5 mM NaCl/0.7 mM NaHCO$_3$. To remove any colloidal goethite particles, the stock was sonicated, centrifuged at 3000 rpm for 1 h (particles < ~100 nm remain suspended),

the supernatant removed and replaced with fresh 5 mM NaCl/ 0.7 mM NaHCO₃, and the process repeated three times.

Each batch sorption experiment was run in duplicate. Samples were prepared by adding the 20 g/L goethite stock to a 5 mM NaCl/0.7 mM NaHCO₃ solution in 50 mL polyethylene tubes to achieve a final solution composition of 0.1 g FeOOH/L. Blank samples containing only goethite in 5 mM NaCl/0.7 mM NaHCO₃ and spiked blank samples containing Np but no goethite were also analyzed. Solutions were allowed to equilibrate for a minimum of 7 days prior to addition of Np. Appropriate quantities of the purified ^{239}Np and ^{237}Np solutions were added to each tube such that samples with low initial Np concentrations (10^{-18}–10^{-15} M) contained pure ^{239}Np, mid range samples (10^{-15}–10^{-11} M) a mixture of ^{239}Np tracer and ^{237}Np (^{237}Np/^{239}Np atom ratio varying from 50 to 5×10^5), and high concentration samples (10^{-9}–10^{-5} M) pure ^{237}Np. In some cases, small amounts of 0.1 M NaOH were added to the samples prior to Np addition. This was performed in order to neutralize any acid from the Np stock.

One hour after Np addition and after each sampling, 100 μL aliquots were collected for pH measurement (Orion Ross semi-microelectrode calibrated with standard pH buffers on an Orion 420A meter). Minor pH adjustments were performed by adding microliter quantities of either HCl or NaOH, as needed. In all but two cases, the pH of each sample was adjusted to be between 7.50 and 7.85, and found to change less than 0.1 pH units throughout the duration of the experiment (Table EA-3).

Samples were mixed continuously using an end-over-end mixer. Sampling was performed at 1, 4–5, and 8 days. At each sampling, tubes were centrifuged at 3000 rpm for 2 h (∼65 nm particle size cutoff). A 5.0 mL aliquot of supernatant was removed from each tube and analyzed by LSC (Packard Tri-Carb TR2900), ICP-MS (XSeries II, Thermo Scientific) and/or gamma spectrometry (Ortec GEM-FX HPGe Coaxial gamma detection system). Pure ^{239}Np and mixed ^{239}Np/^{237}Np samples were analyzed using LSC in cpm counting mode. ^{239}Np counting efficiencies for each sample were determined using a ^{239}Np quenching curve. Care was taken to minimize the spectral window without sacrificing the efficiency, in order to decrease the background as much as possible. Samples containing pure ^{237}Np were counted using LSC in alpha–beta discrimination mode. A high discriminator setting was used to reduce the beta spillover to less than 0.3%. Gamma counting efficiencies for ^{239}Np were determined using a NIST ^{243}Am standard (SRM 4332D). The 277 keV peak was used for ^{239}Np quantification.

Each sample was counted for a total of 2–6 h. Samples containing ^{239}Np were decay corrected to account for ^{239}Np decay during counting time and all sample activities were decay corrected to the time of sampling. Samples were not corrected to account for Np losses in blank samples, as such a correction would not account for competition for Np sorption between goethite and the walls of the reaction vessel [16]. Detection and quantitation limits were defined and calculated using the "paired observations" equations given by Currie [39].

2.3. Modeling

Initial modeling of the sorption data was performed using single site, 2-site, and 3-site models utilizing combinations of linear, Langmuir, and Freundlich isotherms. Combinations of different site types for multi-site models were analyzed in either parallel or consecutive sorption modes as described by Tinnacher et al. [18]. Final optimization of the parameters for the 2-site and 3-site Langmuir models was performed using a modified version of the fitting program FITEQL [40] as described by Zavarin et al. [41]. Each data point was weighted by its uncertainty as calculated from counting results. A minimum error of 3% was assigned to each data point to account for experimental errors in an approximate way (see Table 2).

2.4. Goethite characterization used to estimate reactive site densities

Characterization of the goethite surface was performed using a Philips CM 300 FEG super-twin TEM operating at 300 kV and a FEI Tecnai G^2 X-Twin Scanning Transmission Microscope (STEM) operating at 200 kV. The star-shaped goethite morphology was observed to represent ∼99% of the total volume of goethite, with the other ∼1% observed to have a needle-like morphology (Fig. EA-1). Using the Pbnm space group, the crystalline goethite surface was estimated to be composed of 89.9% ⟨100⟩, 9.1% ⟨010⟩, 0.5% ⟨001⟩, and 0.5% ⟨021⟩ surfaces. More detailed morphological characterization (e.g. corners, edges, defects) was not attempted.

The total surface site density for Np on goethite was not determined radiometrically due to the solubility limit of Np [42]. Instead, a total surface site density of 3.57 sites/nm^2 was estimated based upon analyses of the surface composition of the goethite using TEM in conjunction with calculated site densities for each crystalline face given by Villalobos and Perez-Gallegos [23]. In order to determine the effect of variance in the total number of surface sites upon the modeling results, the total number of sites in the multi-site Langmuir models was allowed to vary from 0.87 to 10.0 sites/nm^2. These site densities were chosen in order to include the upper and lower limits of the expected total site densities reported by Villalobos for bidentate sorption [23,43]. No significant differences were observed in the overall trends as the total site densities were varied (Figs. EA-6 and EA-7). As a result, the density of Type I sites was fixed (with no assigned uncertainty) during the final fitting routine and the errors in the fitted Type II and III site densities represent the error in each of those model parameters as calculated by FITEQL.

3. Results and discussion

3.1. Detection and quantitation limits

Detection limits for several methods currently used for ultralow level environmental Np studies are listed in Table 1. Using ^{239}Np tracers, we are able to measure neptunium concentrations as low as 10^{-18} M using liquid scintillation counting without any sample pre-concentration. While the ^{237}Np detection limits can be significantly improved via pre-concentrating larger sample volumes, this results in higher costs and greater sample preparation time without a significant improvement in the detection limit afforded by ^{239}Np. Additionally, while ^{239}Np offers a relatively simple, inexpensive approach to performing short-term sorption studies, techniques such as accelerator mass spectrometry are invaluable for long-term sorption studies for which the ^{239}Np lifetime would be too short and for ^{237}Np quantitation in environmental samples in which no short half-lived species are present.

Counting of ^{239}Np tracers using liquid scintillation counting yielded a detection limit of 2×10^{-18} M and quantitation limit of 5×10^{-18} M, representing an eight order of magnitude decrease in detection and quantitation limits relative to pure ^{237}Np (1.1×10^{-10} M and 4.0×10^{-10} M respectively). Due to its lower efficiency, the detection and quantitation limits of ^{239}Np using gamma spectroscopy (3×10^{-17} and 1×10^{-16}, respectively) were found to be roughly an order of magnitude higher than those obtained using LSC. While achieving lower Np detection limits is possible, standard commercially available counting system appears to have a practical detection capability of ∼10^{-18}–10^{-17} M. It is important to note that at even lower concentrations, the quantized nature of matter will result is errors due solely to the statistical nature of sampling [44]. In our study, this error was found to be insignificant compared to counting error over the concentration range examined.

Table 1

Detection limits for several analytical methods used in environmental Np research. ^{239}Np tracers enable sorption studies at ultra-low concentrations using purely radiometric techniques.

Method	Sample size (mL)	Nuclide	DL (ppb)	DL (M)	Reference
Liquid scintillation	5.00	^{239}Np	5×10^{-10}	2×10^{-18}	This paper
Gamma spectroscopy	5.00	^{239}Np	8×10^{-9}	3×10^{-17}	This paper
Liquid scintillation	5.00	^{237}Np	2.6×10^{-2}	1.1×10^{-10}	This paper
Accelerator mass spectrometry	5.00	^{237}Np	7×10^{-7}	3×10^{-15}	Brown et al. [45]
ICP-MS	5.00	^{237}Np	6×10^{-3}	3×10^{-11}	Moreno et al. [46]

Table 2

Best fit parameters for the 2-site and 3-site Langmuir models (errors are two sigma error values reported by FITEQL).[a]

	$\text{Log} K_{III}$ (L/mol)	$\text{Log} K_{II}$ (L/mol)	$\text{Log} K_{I}$ (L/mol)	Type III site density (sites/nm^2)	Type II site density (sites/nm^2)	Type I site density (sites/nm^2)	% Type I sites	% Type II sites	% Type III sites
2-Site model	9.13 ± 0.05	N/A	4.98 ± 0.02	$1.6 \times 10^{-3} \pm 0.2 \times 10^{-3}$	N/A	3.57	99.956	N/A	0.044 ± 0.005
3-Site model	10.47 ± 0.08	7.6 ± 0.1	4.85 ± 0.02	$7 \times 10^{-5} \pm 1 \times 10^{-5}$	0.014 ± 0.007	3.56	99.6	0.4 ± 0.1	0.0020 ± 0.0003

[a] The form of the Langmuir equation used herein was $S/S_{max} = KC/(1 + KC)$ where S is the equilibrium sorbed concentration and S_{max} is the maximum sorbed concentration, K is the Langmuir constant (L/mol), and C is the equilibrium aqueous concentration (mol/L).
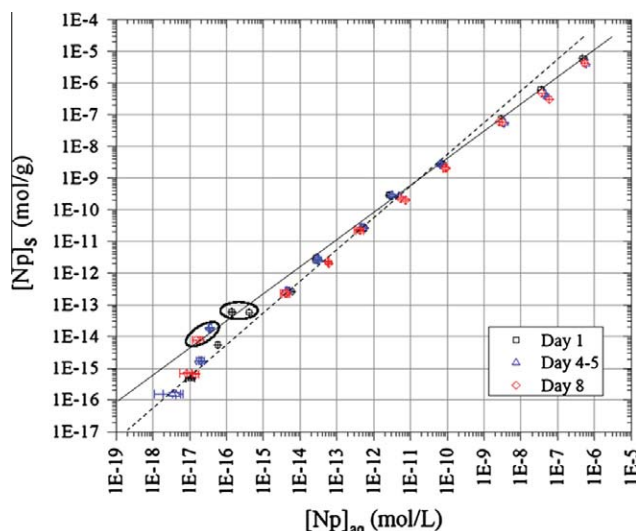
3.2. Sorption isotherm

The Np–goethite sorption isotherm is shown in Fig. 1. No significant changes in the aqueous–solid Np distributions were observed from 1 to 8 days, indicating that equilibrium conditions had been reached within the first day, consistent with previous kinetic studies of Np sorption to goethite [18]. As the equilibrium aqueous Np concentration decreases from $\sim 10^{-5}$ to 10^{-11} M a steady increase in the sorbed/aqueous Np ratio is observed. This behavior is consistent with the Freundlich-like behavior identified by Tinnacher et al. [18]. At aqueous Np concentrations below $\sim 10^{-11}$ M, however, a change in the slope of the isotherm is observed, with the slope approaching a value of 1, indicating linear-like behavior at ultra-low concentrations.

While the trend in the data over the entire concentration range can be represented by a relatively smooth curve, one set of duplicate samples (initial concentration of 10^{-16} M) does not follow this trend. These two samples contained the highest concentrations of pure ^{239}Np and, correspondingly, were originally spiked with large

volumes of acidic ^{239}Np stock solution and required equivalent large quantities of NaOH. In addition, these two samples had consistently low pHs at each sampling and required the addition of NaOH at various times to adjust the pH back to within the desired range of 7.5–7.85 pH units (Table EA-3). These acid/base additions and pH instability appear to have affected Np sorption. As the pH of these samples was not consistent with those of the rest of the experiment, the data are excluded from the modeling effort.

Fig. 2 shows a plot of the surface area normalized K_d as a function of aqueous Np and compares the data obtained in this study to data reported in the literature. Excellent quantitative agreement is observed between this study and values reported by Tinnacher et al. [18], Cromieres [27], Combes et al. [28], and Kohler et al. [29] for Np sorption to synthetic goethite. Surface area normalized K_d values from Nakayama and Sakamoto [30] for Np sorption to natural goethite were slightly lower than those obtained in our study. Nevertheless, the results are remarkably consistent with our synthetic goethite data. To our knowledge, no Np–goethite sorption data are available in the literature at concentrations lower

Fig. 1. Np–goethite sorption isotherm. A change in the slope of the isotherm from a value less than 1 (solid line) to 1 (dashed line) is observed at concentrations lower than $\sim 10^{-11}$ M aqueous Np. Two samples with unstable pHs, as described in the text, are highlighted.
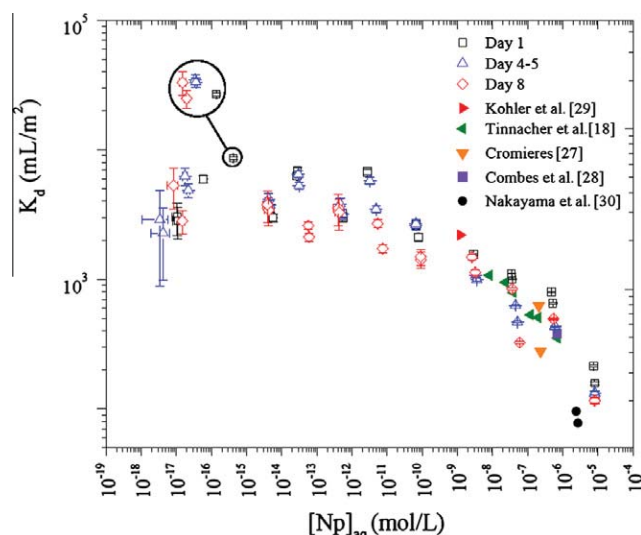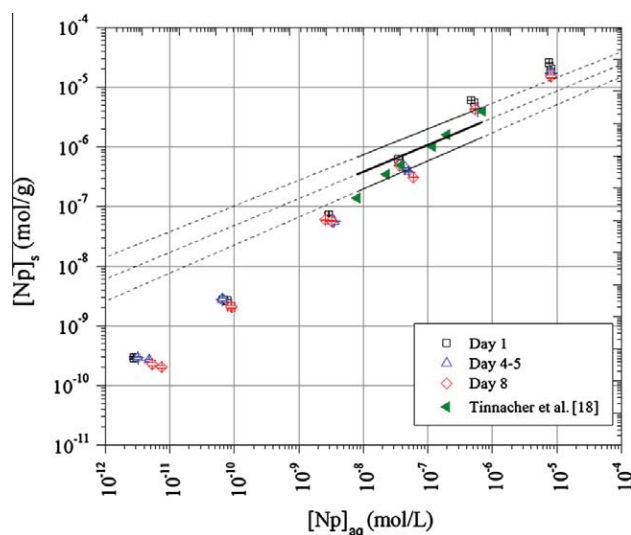

Fig. 2. Comparison of surface area normalized K_d values from the literature to those obtained in this study. Two samples with unstable pHs, as described in the text, are highlighted.

than 10^{-11} M. However, our identification of linear Np–goethite sorption below 10^{-11} M (i.e. constant surface area normalized K_d) is consistent with the linear Np–amorphous iron oxyhydroxide sorption in the 10^{-14}–10^{-12} M concentration range reported by Girvin et al. [13]. However, Girvin et al. [13] did not measure the BET surface area of their solid phase so a quantitative comparison with respect to surface loading is not possible.

The change in the slope of the isotherm (Fig. 1) and change in the surface area normalized K_d (Fig. 2) at ~10^{-11} M indicates a change in Np affinity for the goethite surface at this concentration. From an isotherm modeling perspective, it suggests a transition between two different site "Types." XAFS data of Np on goethite [28] and hematite [43] indicate that Np exists as a monomer on the surface in 6.5×10^{-7} M and 4×10^{-6} M Np solutions respectively. As a result, the observed change in sorption behavior at 10^{-11} M Np is not a product of the formation of polynuclear Np species or surface precipitation [28]. Thus, with the possible exception of the highest concentration sample, it is likely that the observed sorption behavior over the entire concentration range reported here is a monomeric adsorption phenomena.

The highest concentration samples (8×10^{-6} M) analyzed in this experiment were slightly below the expected solubility limit of Np(V) (~2×10^{-5} M as reported by Efurd et al. [42] under similar solution conditions). High-resolution TEM and EDS data, collected several weeks after the sorption experiments were completed, suggest the possible formation of small quantities of Np surface precipitates on goethite (Figs. EA-2 and EA-3). However, these surface precipitates likely account for only a small fraction of the total Np on the surface. As a result, inclusion of surface precipitation or other polynuclear Np sorption processes in our modeling was not considered. Research is currently underway to further evaluate formation of Np nano-colloids on the goethite surface at these very high concentrations.

Fig. 3 compares our isotherm data to the batch sorption data reported in Tinnacher et al. [18] as well as their 2-site consecutive linear-Freundlich model. The linear-Freundlich model was developed from a fit to a flow cell sorption/desorption experiment performed over a concentration of 2×10^{-8}–2×10^{-6} M. Batch sorption data from both studies are in quantitative agreement and, over the 10^{-8}–10^{-6} M range, data from both studies fall within the upper and lower limits of the linear-Freundlich model. As the concentration decreases below 10^{-8} M, the linear-Freundlich model predicts higher K_ds than are experimentally observed. Additionally, the linear-Freundlich model underestimates sorption above 10^{-6} M. Thus, while the linear-Freundlich model adequately predicts batch sorption in the ~10^{-8} to ~10^{-6} M Np range, the model fails to accurately predict batch sorption outside that range. The predictive limitation of the linear-Freundlich model does not invalidate the results from Tinnacher et al. [18]. It simply serves as a reminder that a model is only valid within the range of conditions for which the model calibration was performed. The decreasing K_d at high concentrations as well as the shift to linearity at 10^{-11} M Np could not be effectively modeled with any combination of multi-site models utilizing one or more Freundlich or linear sorption expressions.

The inability of the Freundlich isotherm to model Np sorption at ultra-low concentrations is indicative of a strict limitation to the predictive capability of the Freundlich model for single sorbate–sorbent systems over very large concentration ranges. The Freundlich isotherm can be shown to be numerically equivalent to a Gaussian-like distribution of Langmuir sites [47]. When taken to its lower limit, the exponent in the model (restricted to be <1) necessarily results in the prediction of increasing K_d with decreasing sorbate concentration, the physical interpretation of which suggests the existence of increasingly smaller quantities of increasingly higher affinity sites. For simple binary systems, this yields an unrealistic conceptual model. Our data, as well as those of Girvin et al. [13], indicate that the K_d will become constant at concentrations lower than ~10^{-11} M. Similar observations of Langmuir behavior at low sorbate concentrations for Cd [16,26], Cu, and Zn [26] sorption to amorphous iron oxyhydroxides, as well as contaminant sorption to more crystalline oxides [48] have also been reported in the literature. A more consistent interpretation of these data, using a multi-site sorption model, would suggest that there is a lower limit beyond which Np–goethite sorption behavior becomes dominated by a single site "Type" upon which sorption behaves linearly.

While combinations of Freundlich and linear sorption models were unable to adequately fit the entire isotherm, multi-site models utilizing Langmuir isotherms were successful. Fig. 4 shows the optimized fit for the 2-site Langmuir model. The 2-site Langmuir model captures the change to linearity at concentrations lower than 10^{-11} M while providing "fair" agreement at higher concentrations. However, this model calculates a "high affinity" site density of 0.0016 ± 0.0002 sites/nm^2 (representing 0.044 ± 0.005% of the total surface sites), which is two orders of magnitude lower than typical Type II "high affinity" site densities for iron oxides reported by Dzombak and Morel (for sorption of various cations to hydrous ferric oxide) [21]. If the Type II site density is controlled by the $\langle 001 \rangle$ plane, as observed by Spadini (for Cd^{2+} sorption to goethite and hydrous ferric oxide) [22], an estimate of ~1% for the Type II site density of this goethite is predicted (calculated using surface area data obtained via TEM in this study in conjunction with site density values reported by Villalobos and Perez-Gallegos [23]). When the Type II site density is restricted during fitting to concentrations amenable to the range of expected "high affinity" sites (~0.5–10%) [21], a more consistently increasing K_d is generally obtained at concentrations greater than ~10^{-8} M. However, the slope of the line approaches linearity at concentrations several orders of magnitude higher than 10^{-11} M and thus is unable to accurately describe the entire set of data (Fig. EA-8, Electronic Annex).

The inconsistency between the very low density, "high affinity" site required by the 2-site model and typical Type II site density values reported in the literature led us to investigate the changes that occur with the addition of a third Langmuir site (Fig. 5). While calculating an increasing K_d with decreasing concentration at
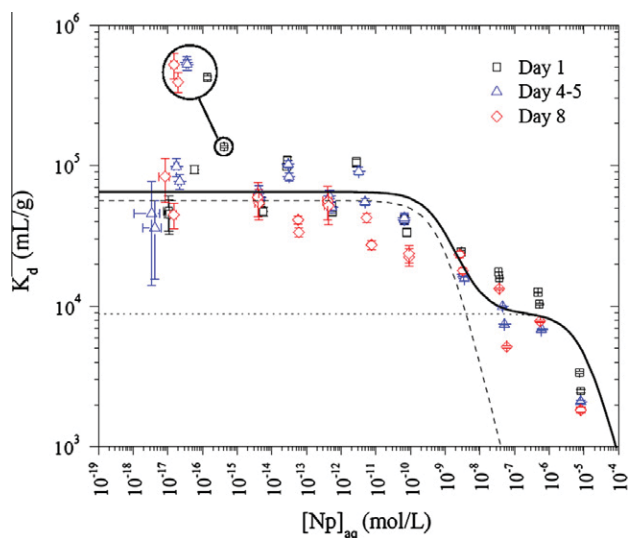

Fig. 3. Comparison of batch sorption data from this study to the batch sorption data and linear-Freundlich model from Tinnacher et al. [18]. Solid lines represent the upper limit, optimal fit, and lower limit parameters reported for the adsorption model, while dashed lines represent the extrapolation of the model to higher and lower concentrations than were examined in Tinnacher et al.'s study.

Fig. 4. Best fit for the 2-site Langmuir model. The 2-site Langmuir model requires the existence of a very low density, high affinity site. Two samples with unstable pHs (highlighted) were not included in the fit.
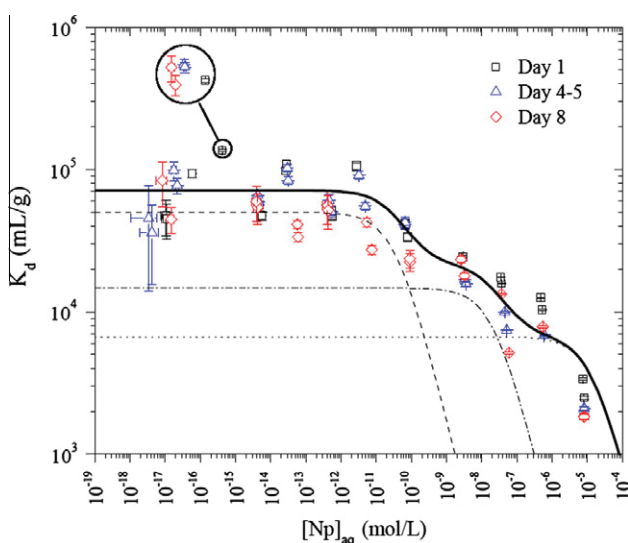
Fig. 5. Best fit for the 3-site Langmuir model. The 3-site model calculates Type II site densities consistent with Dzombak and Morel "high affinity" sites, while also requiring the existence of a very low density of high affinity sites. Two samples with unstable pHs (highlighted) were not included in the fit.

concentrations above 10^{-11} M, the 3-site model calculates a Type II site density of 0.014 ± 0.007 sites/nm^2 (0.4 ± 0.1%), which is within the expected range of Type II site densities reported by Dzombak and Morel [21,22], and is close to our estimated value of ~1% for Type II sites identified based on Cd^{2+} data [22]. As with the 2-site model, the 3-site model requires a very low density, high affinity site ("Type III" site) in order to describe the change to linear sorption behavior at concentrations below 10^{-11} M.

Direct investigation of the nature of the Type III site is complicated by the low concentration at which it is predicted to exist. Isotherm data and associated sorption models, alone, are insufficient to provide mechanistic or structural information. Interestingly, however, Spadini, using EXAFS to study the sorption of Cd^{2+} on goethite at surface loads of 10–100%, reported that cadmium sorption at low surface loading occurred via the sharing of edges and corners with surface iron octahedra in the $\langle 001 \rangle$ plane, whereas at medium and high surface loads sorption occurred primarily along chains on $\langle hk0 \rangle$ planes [22]. While these results, as well as XAS data from Manceau [49] (SeO_3^{2-}, U(VI), Pb(II), and Cr(III) on HFO) and modeling efforts by Villalobos and Perez-Gallegos [23] (H$^+$, Cr(VI), CO_3^{2-}, and Pb(II) on goethite), are able to propose possible identities for typical "low affinity" Type I and "high affinity" Type II sorption sites, their techniques are confined to higher surface loading than are calculated for the Np(V) Type III sites. Direct spectroscopic measurements (e.g. EXAFS) examination at these concentrations is not likely to be possible. However, computational methods may provide a unique opportunity to probe speciation and sorption behavior at these environmentally relevant concentrations [50].

4. Conclusions

The usage of ^{239}Np tracers offers a relatively simple, inexpensive approach for ultra-low level Np sorption studies, and is able to extend the detection limits down to 2×10^{-18} M and 3×10^{-17} M for liquid scintillation counting and gamma spectroscopy respectively. The ultra-low level Np analyses provide a means to study sorption at Np concentrations observed in the environment (10^{-17}–10^{-13} M). Sorption of Np to goethite is observed to reach equilibrium within 1 day, consistent with previous literature studies. At higher concentrations (10^{-5}–10^{-11} M) K_d is observed to increase as the concentration decreases. At concentrations below $\sim 10^{-11}$ M, linear-like sorption behavior is observed. While Freundlich isotherms are able to describe the data in the 10^{-5}–10^{-11} M range, single- and multi-site models employing one or more Freundlich type sites are unable to describe sorption over the entire concentration range analyzed. Both two site and three site Langmuir models are able to describe the data, with the 3-site model resulting in calculated Type I and II site densities consistent with those reported by Dzombak and Morel [21] and estimates based upon observations by Spadini et al. [22] in conjunction with site density values given by Villalobos and Perez-Gallegos [23]. However, both models require the existence of a very low density, high affinity site in order to describe the change in behavior at 10^{-11} M. Thus, interpreted in terms of a multi-site sorption model, our data suggests the existence of a third, previously unidentified type of site that controls Np sorption to goethite at very low surface loads. The nature of this site (e.g. surface defect, impurity, or otherwise) is not known. However, it implies that Np sorption behavior at ultra-low concentrations observed in the field may differ from high Np concentration sorption experiments regularly performed in the laboratory. The underestimated K_d can result in under predicted retardation of the aqueous species and/or under predicted colloid facilitated transport depending on the dominant Np transport mechanism in the field. It is likely that previous studies have not identified such a site's existence as most studies have focused on Np–mineral interactions at much higher concentrations and thus interactions with a low density site would appear masked by Type I and II sites which are of much greater abundance.

Acknowledgments

Appendix A. Supplementary data

Supplementary data associated with this article can be found, in the online version, at http://dx.doi.org/10.1016/j.jcis.2012.08.058.

References

 [1] K.J. Cantrell, Transuranic Contamination in Sediment and Groundwater at the US DOE Hanford Site. PNNL-18640, Pacific Northwest National Laboratory: Richland, WA, 2009.
 [2] A.R. Felmy, K.J. Cantrell, S.D. Conradson, Phys. Chem. Earth 35 (2010) 292–297.
 [3] D.K. Smith, D.L. Finnegan, S.M.J. Bowen, Environ. Radioact. 67 (2003) 35–51.
 [4] T.M. Beasely, J.M. Kelley, T.C. Maiti, L.A.J. Bond, *Environ. Radioact.* 38 (2) (1998) 133–146.
 [5] S.S. Kim, M.H. Baik, K.C.J. Kang, Radioanal. Nucl. Chem. 280 (3) (2009) 577–583.
 [6] J.P. Kaszuba, W.H. Runde, *Environ. Sci. Technol.* 33 (1999) 4427–4433.
 [7] S. Dierking, S. Amayri, T.J. Reich, *Nucl. Sci. Technol.* 6 (2008) 133–137.
 [8] G.R. Choppin, L.F. Rao, Radiochim. Acta 37 (3) (1984) 143–146.
 [9] W. Runde, Los Alamos Sci. 26 (2000) 392–411.
[10] A.B. Kersting, D.W. Efurd, D.L. Finnegan, D.J. Rokop, D.K. Smith, J.L. Thompson, *Nature* 397 (1999) 56–59.
[11] A.B. Kersting, Colloids and radionuclide transport, in: A. MacFarlane, R. Ewing (Eds.), Uncertainty Underground: Yucca Mountain and the Nation's High Level Nuclear Waste, M.I.T. Press, 2006.
[12] A.B. Kersting, M. Zavarin, Colloid-facilitated transport of plutonium at the Nevada test site, NV, USA, in: Stephan N. Kalmykov, Melissa A. Denecke (Eds.), Actinide Nanoparticle Research, Springer, 2011.
[13] D.C. Girvin, L.L. Ames, A.P. Schwab, J.E. McGarrah, J. Colloid Interface Sci. 141 (1) (1991) 67–78.
[14] W.L. Keeney-Kennicutt, J.W. Morse, Mar. Chem. 15 (1984) 133–150.
[15] K. Nakata, S. Nagasaki, S. Tanaka, Y. Sakamoto, T. Tanaka, H. Ogawa, Radiochim. Acta 90 (2000) 665–669.
[16] D.A. Dzombak, J. Colloid Interface Sci. 112 (2) (1985) 588–598.
[17] P.J. Swedlund, J.G. Webster, G.M. Miskelly, Appl. Geochem. 18 (2003) 1671–1689.
[18] R.M. Tinnacher, M. Zavarin, B.A. Powell, A.B. Kersting, Geochim. Cosmochim. Acta 75 (2011) 6584–6599.
[19] C.A.J. Appelo, M.J.J. Van Der Weiden, C. Tournassat, L. Charlet, Environ. Sci. Technol. 36 (2002) 3096–3103.
[20] T.D. Waite, J.A. Davis, T.E. Payne, G.A. Waychunas, N. Xu, Geochim. Cosmochim. Acta 58 (24) (1994) 5465–5478.
[21] D.A. Dzombak, F.M.M. Morel, Surface Complexation Modelling: Hydrous Ferric Oxide, John Wiley, New York, 1990.
[22] L. Spadini, A. Manceau, P.W. Schindler, L. Charlet, J. Colloid Interface Sci. 168 (1994) 73–86.
[23] M. Villalobos, A. Perez-Gallegos, J. Colloid Interface Sci. 326 (2008) 307–323.
[24] P. Venema, T. Hiemstra, W.H. Van Riemsdijk, J. Colloid Interface Sci. 183 (1996) 515–527.
[25] C.M. Eggleston, A.G. Stack, K.M. Rosso, A.M. Bice, Geochem. Trans. 5 (2) (2004) 33–40.
[26] M.M. Benjamin, J.O. Leckie, J. Colloid Interface Sci. 79 (1) (1980) 209–221.
[27] L. Cromieres, Ph.D. Dissertation, Universite de Paris-Sud XI, Orsay, France, 1996.
[28] J. Combes, C.J. Chisholm-Brause, G.E. Brown, G.A. Parks, Environ. Sci. Technol. 26 (1992) 376–382.
[29] M. Kohler, B.D. Honeyman, J.O. Leckie, Radiochim. Acta 85 (1999) 33–48.
[30] S. Nakayama, Y. Sakamoto, Radiochim. Acta 52(3) (1991) 153–157.
[31] P. Zhao, R.M. Tinnacher, M. Zavarin, R.W. Williams, A.B. Kersting, Neptunium Transport Behavior in the Vicinity of Underground Nuclear Tests at the Nevada Test Site, LLNL-TR-464651, 2011.
[32] B.R. Harvey, L.M. Thurston, Aquatic environment protection: analytical methods, MAFF Direct. Fish. Res. Lowestoft, 1988, pp. 1–36.
[33] S. Rollin, H. Sahli, R. Holzer, M. Astner, M. Burger, Appl. Radiat. Isot. 67 (2009) 821–827.
[34] J.A. Veith, G. Sposito, Soil Sci. Soc. Am. J. 41 (4) (1977) 697–702.
[35] G. Limousin, J.-P. Gaudet, L. Charlet, S. Szenknect, V. Barthes, M. Krimissa, Appl. Geochem. 22 (2007) 249–275.
[36] U. Schwertmann, R.M. Cornell, Iron Oxides in the Laboratory: Preparation and Characterization, VCH Verlagsgesellschaft mbH, Weinheim, 1991.
[37] David A. Pickett, Michael T. Murrell, Ross W. Williams, Anal. Chem. 66 (1994) 1044–1049.
[38] Robert Guillaumont, Thomas Fanghanel, Jean Fuger, Ingmar Grenthe, Volker Neck, Donald A. Palmer, Malcolm H. Rand, Update on the Chemical Thermodynamics of Uranium, Neptunium, Plutonium, Americium, and Technetium, Elsevier, Amsterdam, 2003.
[39] Lloyd A. Currie, Anal. Chem. 40 (3) (1968) 586–593.
[40] A.L. Herbelin, J.C. Westall, FITEQL: A Computer Program for Determination of Chemical Equilibrium Constants from Experimental Data, Department of Chemistry, Oregon State University, USA, 1994.
[41] M. Zavarin, S.K. Roberts, N. Hakem, A.M. Sawvel, A.B. Kersting, Radiochim. Acta 93 (2005) 93–102.
[42] D. Wes Efurd, Wolfgang Runde, Joe C. Banar, David R. Janecky, John P. Kaszuba, Phillip D. Palmer, Fred R. Roensch, C. Drew Tait, Environ. Sci. Technol. 32 (1998) 3893–3900.
[43] Arai Yuji, P.B. Moran, B.D. Honeyman, J.A. Davis, Environ. Sci. Technol. 41 (2007) 3940–3944.
[44] Constantinos E. Efstathiou, Talanta 52 (2000) 711–715.
[45] T.A. Brown, A.A. Marchetti, R.E. Martinelli, C.C. Cox, J.P. Knezovich, T.F. Hamilton, Nucl. Instrum. Methods Phys. Res. Sect. B 223–224 (2004) 788–795.
[46] J.M. Barrero Moreno, M. Betti, J.I. Garcia Alonso, J. Anal. At. Spectrom. 12 (1997) 355–361.
[47] Robert Sips, J. Chem. Phys. 16 (5) (1948) 490–495.
[48] M.M. Benjamin, J.O. Leckie, Ann Arbor Sci. 2 (1980) 305–322 (Chapter 16).
[49] A. Manceau, L. Charlet, M.C. Boisset, B. Didier, L. Spadini, Appl. Clay Sci. 7 (1992) 201–223.
[50] Patrick Huang, Mavrik Zavarin, Annie B. Kersting, Chem. Phys. Lett. 543 (2012) 193–198.